Interplay of One- and Two-Step Channels in Electrovibrational Two-Photon Absorption

S. Polyutov,* I. Minkov, F. Gel'mukhanov, and H. Ågren

Theoretical Chemistry, Roslagstullsbacken 15, Royal Institute of Technology, S-106 91 Stockholm, Sweden

Received: July 1, 2005; In Final Form: September 2, 2005

We present a theory of two-photon absorption that addresses the formation of spectral shapes taking the vibrational degrees of freedom into account. The theory is used to rationalize the observed differences between the spectral shapes of one- and two-photon absorption. We find that the main cause of these differences is that the two-step and coherent two-photon spectral bands are different even considering a single final state. Our formalism is applied to the N101 molecule (*p*-nitro-*p*′-diphenylamine stilbene), which was recently studied experimentally. Simulations show that the two-step two-photon electrovibrational absorption results in a blue shift of the absorption spectrum in agreement with the measurements.

1. Introduction

Understanding the formation of two-photon spectra is essential in order to tailor structure−property relations for two-photon materials and improve their use in technical applications. Two-photon absorption (TPA) of polyatomic molecules is influenced strongly by vibrational interaction, providing a general broadening of the spectra with fine structure. As for other types of electronic transitions, this merely reflects the fact that the potential surface changes when going from the ground to the final state of the optical excitation. The conventional theory of two-photon absorption based on the one-step model describes the vibrational profile through the Franck−Condon (FC) factors between the ground and the final state.[1,2] This means that the two-photon profile copies the profile of one-photon absorption corresponding to the same electronic transition as a consequence of the fact that the Franck−Condon principle is exactly the same for the two processes. However, experiments, for example, refs 3 and 4, indicate a strong violation of this statement. The aim of this article is to explain the reason for this phenomenon. Our approach is based essentially on the dynamical theory developed in our previous articles.[8−12] The key idea is that the conventional coherent TPA (one-step absorption) is accompanied by two-step TPA. The latter process has the same order of magnitude as the one-step absorption, because the suppression of TPA by off-resonant population of the first excited state is compensated by resonant excited-state absorption. The main reason for the profile differences of one- and two-step TPA is that, contrary to the coherent channel, the vibrational profile of the two-step TPA is given by the FC factors between the first and higher excited electronic state. Considering the full many-state spectra, one- and two-photon absorption also differ because of the trivial fact that the set of excited electronic states have different relative cross-sections for the one- and two-photon processes.

The article is organized as follows. We start in Section 2 describing the theoretical model of TPA. The computational details are elucidated in Section 3. We analyze the obtained one-photon and two-photon absorption spectra in Section 4. Our findings are summarized in Section 5.

* Corresponding author. E-mail: sergey@theochem.kth.se.

2. Formulation of the Theory

The conventional theory of TPA absorption is based on the one-step model of TPA. To explain the distinction between the vibrational profiles of one- and two-photon absorption, we also take the two-step TPA channel into account. Two-step TPA consists of nonresonant one-photon population of the electronic level, *i*, with forthcoming one-photon resonant excited-state absorption $i \rightarrow \alpha$ (Figure 1). We consider the nonlinear interaction of the optical field with a many-level molecule. This optical field, **E**, induces a nonlinear polarization, **P**:

$$\mathbf{E} = \frac{\mathcal{E}}{2}e^{-\iota\omega+\iota kz} + \text{c.c.} \quad \mathbf{P} = \text{P}e^{-\iota\omega+\iota kz} + \text{c.c.} \quad k = \frac{\omega}{c} \tag{1}$$

Extraction of the fast variables in the Maxwell equations results in the following paraxial wave equation:

$$\left(\frac{\partial}{\partial z} + \frac{1}{c}\frac{\partial}{\partial t} - \frac{\iota}{2k}\Delta_{\perp}\right)\mathcal{E} = \frac{\iota k}{\epsilon_0}\text{P} \tag{2}$$

The SI system of units is used here. We will neglect the transverse inhomogeneity of the light beam, $\Delta_{\perp}\mathcal{E} \simeq 0$, in order to focus our attention on the main effects. This leads to the following equation for the light intensity, $I = c\epsilon_0|\mathcal{E}|^2/2$:

$$\left(\frac{\partial}{\partial z} + \frac{1}{c}\frac{\partial}{\partial t}\right)\text{I} = -kc\,\mathcal{I}m(\mathcal{E}^*\text{P}) \tag{3}$$

To find the polarization of the system shown in Figure 1

$$\mathbf{P} = Tr\,(\mathbf{d}\rho) = 2\mathbb{R}e[\mathbf{d}_{0i}\rho_{i0} + \sum_{\alpha}(\mathbf{d}_{\alpha 0}\rho_{0\alpha} + \mathbf{d}_{\alpha i}\rho_{i\alpha})] \tag{4}$$

we need to know the transition dipole moments, $\mathbf{d}_{ij}$, and the density matrix, ρ, of the absorber.

2.1. Shape of the Spectral Line and the Relaxation Constants. The relative intensity of two-step TPA depends strongly on the spectral shape of the wings of one-photon absorption. This makes it instructive to overview the spectral line shape and the time hierarchy. The spectral shape of photoabsorption of a solute (molecular chromophore) in a solvent experiences two qualitatively different broadening mechanisms, namely, homogeneous and inhomogeneous broadenings.[15,16] Both mechanisms of broadenings are also accompanied by blue

10.1021/jp0536100 CCC: $30.25
Published on Web 10/05/2005

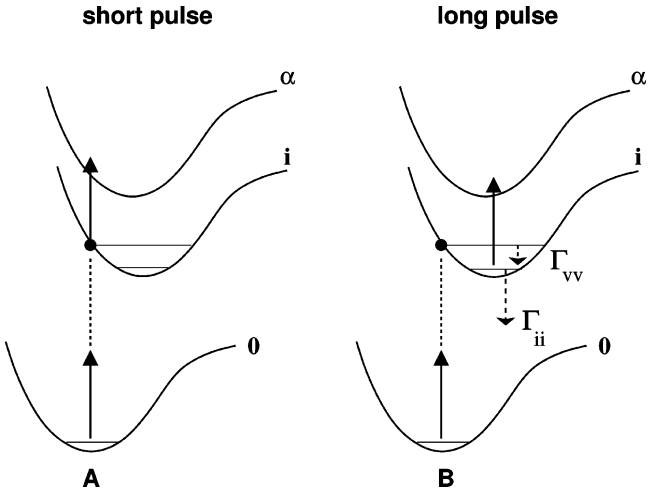

Figure 1. Scheme of two-step TPA transitions.

or red shifts of the optical bands. Homogeneous line broadening is essentially a dynamical process caused by collisions between solute and solvent, which are sufficiently fast to affect different chromophores in the same way. The notion of collisional broadening, which comes from gas-phase spectroscopy, can also be used in the condensed phase. More strictly, one can speak about dynamical broadening caused by acoustic phonon-like motion of the solvent.

Static or inhomogeneous broadening arises because of the fact that the resonant frequency of the chromophore is different in different local environments.[14] The question of which broadening mechanism is the dominating one is far from clear (compare refs 15−17). Both the solute and solvent molecules in the discussed experiment[3] have rather large permanent dipole moments; the solvent molecule, tetrahydrofuran (THF), possesses a dipole moment of 1.63 D. Because of this circumstance, the dipole−dipole interaction is responsible for the two broadening mechanisms for the studied system. The origin of the homogeneous and inhomogeneous broadenings is the same: it is the change of the permanent electric dipole moment, $\Delta\mathbf{d}_{ii} = \mathbf{d}_{ii} - \mathbf{d}_{00}$, upon electronic excitation $0 \rightarrow i$. This means that the electrovibrational line experiences larger broadening for electronic transitions with a larger change of the permanent dipole moment.

The spectral line shape deviates strongly from a Lorentzian shape because of the dynamical and static interaction with the solvent. Namely, the one-photon absorption probability, $P_{ij}(\omega)$, drops down essentially faster than a Lorentzian at the red wing of the spectral line.[13] Such a deviation is accounted for in our approach by the frequency-dependent "width"

$$\Gamma_{ij}(\omega) = \frac{1}{2}(\Gamma_{ii} + \Gamma_{jj}) + \gamma_{ij}(\omega). \qquad (5)$$

The decrease of $\Gamma_{ij}(\omega)$ at the wings of the spectral line is essential for the estimation of the role of the two-step TPA channel. To estimate the off-resonant population of the first excited-state, we use experimental data (see Section 3).

A few characteristic time scales govern the dynamics of the studied system: the pulse duration, τ, the lifetimes of the excited electronic states, Γ_{ii}^{-1}, the lifetime of the vibrational state, $\Gamma_{VV}^{-1} \lesssim 1$ ps,[6,7] and the lifetime, $\Gamma_{ij}^{-1}(\omega)$, of the coherence, ρ_{ij} ($i \neq j$). To be specific, we will consider only the collisional broadening. The decay rate (eq 5) of the coherence consists of two qualitatively different contributions; the first contribution is related to the decay rates, Γ_{ii} and Γ_{jj}, of the i and j states' population. Near the resonance, $\omega \approx \omega_{ij}$, the dephasing rate, $\gamma_{ij}(\omega)$, is proportional to the total concentration, N_{tot}, of molecules in the solution: $\gamma_{ij}(\omega_{ij}) \simeq \bar{v}\sigma_{ij}N_{\text{tot}}$, where σ_{ij} is the cross section of the dephasing collisions of the absorbing molecule with the solvent particles and $\bar{v}$ is the thermal velocity. It is striking that the expression for $\gamma_{ij}(\omega_{ij})$, being valid strictly for the gas phase, gives the correct order of magnitude even for liquids:[13] $\Gamma_{ij}(\omega_{ij}) \approx \gamma_{ij} \approx 0.1-0.01$ eV ($1/\gamma_{ij}(\omega_{ij}) \approx 7-70$ fs). When the detuning from resonant frequency is larger than the inverse duration of collision, $|\omega - \omega_{ij}| \gg \tau_{\text{coll}}^{-1}$, the collisional broadening, $\gamma_{ij}(\omega)$, drops down. Because of this, the one-photon absorption at the wings of the spectral line, $P_{ij}(\omega) \approx \Gamma_{ij}(\omega)/(\omega - \omega_{ij})^2$, decays faster than a Lorentzian (see Section 2.3).

The decay rate, Γ_{ii}, of population ρ_{ii} is determined mainly by the intramolecular radiative, Γ_{ii}^{r}, and nonradiative (internal conversion), Γ_{ii}^{nr}, transitions: $\Gamma_{ii} = \Gamma_{ii}^{\text{r}} + \Gamma_{ii}^{\text{nr}}$. Optical experiments[18] with organic molecules show that the lowest excited electronic state has the longest lifetime $\Gamma_{11}^{-1} \approx 1$ ns ($\Gamma_{11} \sim 0.7 \times 10^{-3}$ meV). The picture differs qualitatively for the higher electronic states, α, which have short lifetimes, in the order of $\Gamma_{\alpha\alpha}^{-1} \lesssim 1$ ps $\ll \Gamma_{11}^{-1}$ ($\Gamma_{\alpha\alpha} \simeq \Gamma_{\alpha\alpha}^{\text{nr}} \gtrsim 0.7$ meV) owing to cascades of nonradiative internal conversions to the lowest excited state.

The theory presented below is developed for pulse duration lying in the interval

$$r \gtrsim \Gamma_{VV}^{-1} > \Gamma_{10}^{-1}(\omega_{10}), |\omega - \omega_{10}|^{-1}. \qquad (6)$$

The pulse duration $\tau = 0.85$ ps used in the experiment[3−5] satisfies this requirement. This time hierarchy (eq 6) essentially simplifies the solution of the kinetic equations for populations and off-diagonal elements of the density matrix

$$\left(\frac{\partial}{\partial t} + \Gamma_{ii}\right)\rho_{ii} = \sum_{\alpha}\tilde{\Gamma}_{\alpha\alpha}\rho_{\alpha\alpha} + \frac{\iota}{\hbar}[\rho, V]_{ii},$$
$$\left(\frac{\partial}{\partial t} + \Gamma_{\alpha\alpha}\right)\rho_{\alpha\alpha} = \frac{\iota}{\hbar}[\rho, V]_{\alpha\alpha}, \quad \left(\frac{\partial}{\partial t} + \Gamma_{ij}(\omega)\right)\rho_{ij} = \frac{\iota}{\hbar}[\rho, V]_{ij}, \quad \text{Tr}\rho = \mathcal{N}, \quad V = -\mathbf{Ed} \qquad (7)$$

where the concentration of the absorbing molecules is denoted by $\mathcal{N}$. Here we neglect the spatial derivatives at the left-hand side of the kinetic equations, which are responsible for the Doppler effect. The Doppler broadening in the studied condensed absorber is indeed negligible compared to the dephasing rate, $\Gamma_{ij}(\omega)$. Because of nonradiative conversion, the rate, $\tilde{\Gamma}_{\alpha\alpha}$, of decay transitions $\alpha \rightarrow i$ is large in organic molecules and almost completely coincides with the total decay rate, $\Gamma_{\alpha\alpha}$. After selection of the fast time variables, $\exp(\pm\iota(\omega \pm \omega_{ij})t)$, the condition (eq 6) allows us to neglect the time derivatives in the equations for the off-diagonal elements, ρ_{ij}. However, the equations for the population must be integrated explicitly.

2.2. Photoabsorption Cross Sections. Using standard techniques and the above statement about the time derivatives, we solve the density matrix equations (eq 7) and find the total polarization including one-photon ($\sim\mathcal{E}$) and two-photon ($\sim|\mathcal{E}|^2\mathcal{E}$) contributions. The final equation for the intensity, or irradiance, is the following:

$$\left(\frac{\partial}{\partial z} + \frac{1}{c}\frac{\partial}{\partial t}\right)I = -\mathcal{N}(\sigma I + \sigma^{(2)}I^2) \qquad \sigma^{(2)} = \sigma_1^{(2)} + \sigma_2^{(2)} \qquad (8)$$

The first term at the right-hand side of eq 8 describes one-photon photoabsorption with a cross-section

$$\sigma = \frac{k}{3\hbar\epsilon_0}\sum_i \frac{d_{i\,0}^2\Gamma_{i\,0}(\omega)\langle 0_0|\nu_i\rangle^2}{(\omega-\omega_{i\nu i,00})^2+\Gamma_{i\,0}^2(\omega)}. \quad (9)$$

Because of the interaction of the absorbing molecules with the solvent, the spectral profile deviates from a Lorentzian through the frequency dependent broadening, $\Gamma_{i0}(\omega)$ (see Sections 2.1 and 3). The total TPA cross-section, $\sigma^{(2)}$, is a sum of a coherent, or one-step ($\sigma_1^{(2)}$), and two-step ($\sigma_2^{(2)}$) contributions.[8,9]

$$\sigma_1^{(2)} = \frac{k}{c\epsilon_0^{\,2}\hbar^3}\sum_i\langle S_{i\,0}\rangle\sum_{\nu_i}\frac{\Gamma_{i\,0}(2\omega)\langle 0_0|\nu_i\rangle^2}{(2\omega-\omega_{i\nu_i,00_0})^2+\Gamma_{i\,0}^2(2\omega)}$$

$$\langle S_{i0}\rangle = \frac{1}{15}\sum_{nm}(s_{nn}s_{mm}+s_{nm}s_{nm}+s_{nm}s_{mn})$$

$$s_{mn} = \sum_\alpha \frac{d_{i\alpha}^{(m)}\,d_{\alpha 0}^{(n)}}{\omega-\omega_{\alpha 0}} + \frac{d_{i\,0}^{(m)}\Delta d_{ii}^{(n)}}{2(\omega-\omega_{i0})} \quad (10)$$

The two-step TPA process consists of the nonresonant population of the vibrational state $|\nu_i\rangle$ of electronic state i followed by resonant excited-state absorption, $i \rightarrow \alpha$. In case the pulse duration, τ is shorter than the lifetimes of the vibrational state ($\tau_{\rm vib} \equiv \Gamma_{VV}^{-1} \approx 1$ ps) and of the electronic state (Γ_{ii}^{-1}), the cross-section of the two-step TPA process reads:

$$\sigma_2^{(2)} = \frac{k}{c\epsilon_0^{\,2}\hbar^3}\sum_{\alpha,\nu_\alpha;i,\nu_i} d_{i\,0}^2 d_{\alpha i}^2 \Lambda_{i\alpha}^{i\,0} P_{i\,0}(\omega)$$

$$\frac{\Gamma_{\alpha i}(\omega)\langle 0_0|\nu_i\rangle^2\langle\nu_i|\nu_\alpha\rangle^2}{[(\omega-\omega_{\alpha\nu_\alpha,i\nu_i})^2+\Gamma_{\alpha i}^{\,2}(\omega)]}\tau^2\Gamma_{VV}, \quad \tau\Gamma_{VV}\ll 1 \quad (11)$$

One can see that the cross-section is proportional to the Franck−Condon factors of the ground state $\langle 0_0|\nu_i\rangle^2$ and excited state $\langle\nu_i|\nu_\alpha\rangle^2$ absorption. This is because the vibrational state, $|\nu_i\rangle$, has no time to decay in the lowest vibrational state, $|0_i\rangle$, of the ith level (Figure 1).

The molecule has time to relax to the lowest vibrational state of the ith electronic state in the case of a longer pulse, $\tau > \tau_{\rm vib}$ and the two-step contribution

$$\sigma_2^{(2)} = \frac{k}{c\epsilon_0^{\,2}\hbar^3}\sum_{i,\alpha,\nu_\alpha} d_{i\,0}^2 d_{\alpha i}^2 \Lambda_{i\alpha}^{i\,0} P_{i\,0}(\omega)$$

$$\frac{R_{ii}}{\Gamma_{ii}}\frac{\Gamma_{\alpha i}(\omega)\langle 0_i|\nu_\alpha\rangle^2}{(\omega-\omega_{\alpha\nu_\alpha,i\,0_i})^2+\Gamma_{\alpha i}^{\,2}(\omega)} \quad (12)$$

depends now on only the FC factor $\langle 0_i|\nu_\alpha\rangle^2$ of excited-state absorption from the bottom of the excited-state potential (Figure 1). We introduced the spectral profile of nonresonant absorption, $P_{i0}(\omega)$, and the anisotropy factor, $\Lambda_{i\alpha}^{\beta 0}$:

$$P_{i\,0}(\omega) = \Gamma_{i0}(\omega)\left[\frac{1}{(\omega-\omega_{i\,0}^V)^2+\Gamma_{i\,0}^2(\omega)}+\frac{1}{(\omega+\omega_{i\,0}^V)^2}\right]$$

$$\Lambda_{i\alpha}^{\beta 0} = \frac{1+2\cos^2(\mathbf{d}_{\beta 0},\mathbf{d}_{i\alpha})}{15} \quad (13)$$

Here, $\mathbf{d}_{i\alpha}$ is the transition dipole moment between electronic states i and α; ω_{i0}^V is the frequency of vertical transition between the ground and excited states, i; $\omega_{\alpha\nu_\alpha,i\nu_i}$ is the frequency of electron-vibrational transition $|i\nu_i\rangle \rightarrow |\alpha\nu_\alpha\rangle$; and $\langle\nu_i|\nu_\alpha\rangle$ is the FC amplitude between multimode vibrational states ν_i and ν_α of electronic states i and α.

The off-resonant population of the ith excited state

$$\rho_{ii} = \frac{\mathcal{N}\mathrm{d}_{i\,0}^2 P_{i\,0}(\omega)}{3\epsilon_0 c\hbar^2\Gamma_{ii}}R_{ii}I \quad (14)$$

depends strongly on the magnitude of the pulse duration and the lifetime of the excited state:[8]

$$R_{ii} \approx 1-\mathrm{e}^{-\tau\Gamma_{ii}} = \begin{cases}\tau\Gamma_{ii}, & \tau\Gamma_{ii}\ll 1\\ 1, & \tau\Gamma_{ii}\gg 1\end{cases} \quad (15)$$

In the simulations presented below, we assume that the pulse is rather long and the molecule has time to relax to the lowest vibrational level of the electronic state, i. The analysis of the time hierarchy (Section 2.1) indicates that this condition is satisfied only approximately: $\tau\Gamma_{VV} \approx 1$.

2.3. Relative Contribution of the Two-Step and the Coherent TPA Channels. The conventional theory of TPA takes into account only the coherent, or one-step, cross-section (eq 2) and ignores completely the sequential two-step TPA. Such an approximation is motivated by the small probability of nonresonant population of the first excited state, $\rho_{11} \propto P_{10} \propto \Gamma_{10}(\omega)(\omega-\omega_{10})^{-2}$, which decays faster than a Lorentzian because of the decrease of $\Gamma_{10}(\omega)$ at the red wing of the spectral line, $\omega = \omega_{10}/2$. However, the one-step TPA is also suppressed by the Lorentzian $\langle S_{10}\rangle \propto (\omega-\omega_{10})^{-2}$. Because of this circumstance and resonant excited-state absorption (Figure 1), the one- and two-step TPA cross-sections can be comparable. This motivates us to write down an accurate estimate for the ratio of these cross sections. Let us note that the major contribution to the coherent cross-section of charge-transfer molecules is due to change of the permanent dipole moment (see the second term in eq 10 for s_{mn}. Equations 10 and 12 give the following estimation:

$$\frac{\sigma_2^{(2)}}{\sigma_1^{(2)}} \approx 4\left(\frac{d_{\alpha 1}}{\Delta d_{11}}\right)^2 \times \frac{P_{10}(\omega)(\omega-\omega_{10})^2}{\Gamma_{11}} \times R_{11} \times \frac{\Gamma_{10}^{\rm R}}{\Gamma_{\alpha 1}^{\rm R}} \approx$$

$$4\left(\frac{d_{\alpha 1}}{\Delta d_{11}}\right)^2 \times \frac{R_{11}\Gamma_{10}^{\rm NR}}{\Gamma_{11}} \times \frac{\Gamma_{10}^{\rm R}}{\Gamma_{\alpha 1}^{\rm R}} \quad (16)$$

Here, $\Gamma_{10}^{\rm R} \equiv \Gamma_{10}(\omega_{10})$ and $\Gamma_{\alpha 1}^{\rm R} = \Gamma_{\alpha 1}(\omega)$ are the values of the broadenings near the resonances of the Lorentzians at the right-hand side of eqs 10 and 12, respectively; $\Gamma_{10}^{\rm NR} \equiv \Gamma_{10}(\omega_{10}/2)$ is the nonresonant value of $\Gamma_{10}(\omega)$ in the probability (eq 13) of nonresonant population of the first electronic state, $P_{10}(\omega)$.

According to our simulations (Table 1) $(d_{\alpha 1}\Delta d_{11})^2 \approx 10^{-2}$. Let us estimate $\Gamma_{10}^{\rm NR}$ making use of the experimental data for Rhodamin B in ethanol[19] for the ratio of nonresonant to resonant absorption in the vicinity of $\lambda = 900$ nm: $P_{10}^{\rm NR}/P_{10}^{\rm R} \approx 10^{-4}$. However, eq 13 means that $P_{10}^{\rm NR}/P_{10}^{\rm R} = \Gamma_{10}^{\rm R}\,\Gamma_{10}^{\rm NR}/(\omega-\omega_{10})^2$. For $\Gamma_{10}^{\rm R} \approx 0.03$ eV and $\omega_{10}-\omega \approx 1.5$ eV (see Section 3), we get $\Gamma_{10}^{\rm NR} \approx 0.008$ eV.

The pulse used in the experiment[3] ($\tau = 0.85$ ps) was much shorter than the lifetime of the first excited state, $\Gamma_{11}^{-1} \approx 1$ ns. Because of this fact, the efficiency (eq 15) of the nonresonant population of this electronic state is suppressed by the factor

TABLE 1: Transition ($d_{\alpha i}$) and Permanent (d_{00}, $\Delta d_{ii} = d_{ii} - d_{00}$) Dipole Moments (in au) of N101

	X	*Y*	*Z*
d_{10}	3.761	−0.132	−0.049
d_{40}	0.119	−1.145	0.017
d_{21}	0.117	0.031	0.097
d_{31}	0.162	0.003	0.002
d_{41}	−0.011	−0.286	−0.007
d_{51}	0.028	−0.161	−0.017
d_{00}	2.832	0.112	0.097
Δd_{11}	−1.940	0.005	0.002
Δd_{22}	−0.124	−0.054	−0.02
Δd_{33}	−1.150	0.044	0.002
Δd_{44}	0.947	−0.016	0.001
Δd_{55}	−0.330	−0.056	−0.036

TABLE 2: Two Sets of Broadening Parameters ($\Gamma^R_{\alpha i}$) near the Resonance Region Used in Our Simulations

	Γ^R_{10}	Γ^R_{40}	Γ^R_{21}	Γ^R_{31}	Γ^R_{41}	Γ^R_{51}
set 1 (eV)	0.01	0.01	0.01	0.01	0.01	0.01
set 2 (eV)	0.05	0.025	0.04	0.02	0.08	0.04

TABLE 3: Vertical Excitation Energies (in eV) of the First Five Excited States of N101[a]

excited state	1	2	3	4	5
ω_{i0} (eV)	3.01	4.06	4.12	4.21	4.3

[a] These transition energies are lowered by 1.214 eV in order to match the experimental value[3] $\omega_{10} = 3.01$ eV.

(eq 15) $R_{11} \approx \tau\Gamma_{11} \ll 1$. This results in $R_{11}\Gamma^{NR}_{10}/\Gamma_{11} \approx \tau\Gamma^{NR}_{10} \approx 10$. Taking into account that $\Gamma^R_{10}/\Gamma^R_{\alpha 1} \approx 1$ (Section 3) we finally conclude that even for rather short pulses ($\tau = 0.85$ ps) the two-step and coherent channels give comparable contributions to the total TPA cross-section: $\sigma^{(2)}_2/\sigma^{(2)}_1 \approx 1$.

3. Computational Details

All of the needed quantities were calculated using the DALTON suite of programs.[21] Our simulations are based on the response theory in the framework of the Hartree−Fock (HF) method. The quadratic response formalism is used in calculations of the dipole moments of transitions between excited states as well as for their permanent dipole moments. The cc-pVDZ basis set was used throughout the simulations. The gap, ω_{10}, between the first excited and the ground state obtained in the HF response method is 4.224 eV, which is higher than the value obtained using time-dependent density functional theory (TDDFT) with the B3LYP functional, 2.52 eV. It is established that the HF method overestimate ω_{10}, whereas the DFT technique produces a value smaller than the experimental one. Because of this, we lowered the HF excited-state energies (Table 3) by 1.214 eV to match the experimental value of the first transition: $\omega_{10} = 3.01$ eV (see Figure 3). All of the quantities were calculated in the ground-state optimized geometry. We take into account the first five excited electronic states with the coherent TPA channel $0 \rightarrow 1$. The analysis of the transition dipole moment shows that the two-step TPA channel $0 \rightarrow 1 \rightarrow \alpha$ dominates.

The many-mode FC amplitudes were computed in the framework of the Born−Oppenheimer approximation as the product of the FC amplitudes of each normal mode, q

$$\langle \nu_i | \nu_\alpha \rangle = \langle \nu_{i,1} | \nu_{\alpha,1} \rangle \langle \nu_{i,1} | \nu_{\alpha,2} \rangle \cdots \langle \nu_{i,N} | \nu_{\alpha,N} \rangle \qquad (17)$$

Here, $\nu_i = (\nu_{i,1}, \nu_{i,2}, \nu_{i,3} \ldots, \nu_{i,N})$ is the vector of the vibrational quantum numbers $\nu_{i,q} = 0, 1, 2, \ldots$ of the qth vibrational normal mode in the ith electronic state.

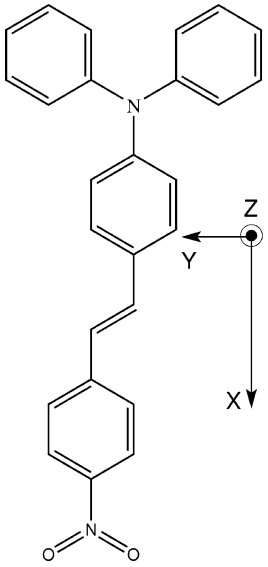

Figure 2. *p*-nitro-*p*′-diphenylamine stilbene (N101) molecule.

The FC factor of the qth mode is calculated in the harmonic approximation through the Huang−Rhys (HR) parameter:

$$\langle 0_{i,q} | \nu_{a,q} \rangle^2 = \frac{S_q(i\alpha)}{\nu_{a,q}!} e^{-S_q(i\alpha)} \qquad S_q(i\alpha) = \frac{F^2_q(i\alpha)}{2\omega^3_q} \qquad (18)$$

The HR parameter is expressed via the gradient of the transition energy $E_\alpha - E_i$ in the equilibrium geometry of the ground electronic state: $F_q(i\alpha) = \partial(E_\alpha - E_i)/\partial Q_q$. We assumed that the vibrational frequencies, ω_q, do not change under electronic excitation.

The explicit treatment of all vibrational modes makes the computations very expensive. To be able to calculate the TPA cross-sections, we selected the more important modes with the HR parameter $S_q(i\alpha) > 0.1$; these are collected in Table 4. These modes can be divided in a few groups: mode 66 corresponds to the C−C−C bending in the phenyl-amino rings; symmetric C−C−H bending is given by modes 86, 88, 90, and 92; modes 93, 100, and 105 correspond to the symmetric C−C−H bending + C−N stretching in the amino group; modes 119, 121, and 122 correspond to the C−C stretching in all aromatic rings; mode 123 is the C−C stretching of the stilbene double bond.

The intensity of the single spectral component incident on the sample was around 1 GW/cm^2. According to estimations, this experimental value is smaller than the saturation intensity. Because of this circumstance, the saturation effects are neglected in the simulations. As was pointed out above, the intensity of the two-step TPA depends on the parameter $\Gamma^{NR}_{10}\tau$, which is assumed in our simulations to be $\Gamma^{NR}_{10}\tau = 10$ (see Section 2.3).

The broadening of the spectral lines deserves a special comment. In the simulations, we assumed that there were two sets of spectral line broadenings near the resonance region, as displayed in Table 2: (1) the same broadening for all spectral transitions and (2) different broadening parameters. The motivation for using different broadenings for different electronic transitions is the following. As was mentioned above, the major cause of the static and dynamical broadenings is the change of the dipole−dipole interaction between solute and solvent molecules during the electronic transition. The broadening of the electrovibrational line $i \rightarrow \alpha$ is defined by the change of the permanent dipole moment $\Delta d(\alpha i) = d_{\alpha\alpha} - d_{ii}$ following the electronic transition $i \rightarrow \alpha$. According to Table 1, these changes are different for different electronic transitions: $\Delta d(10)$

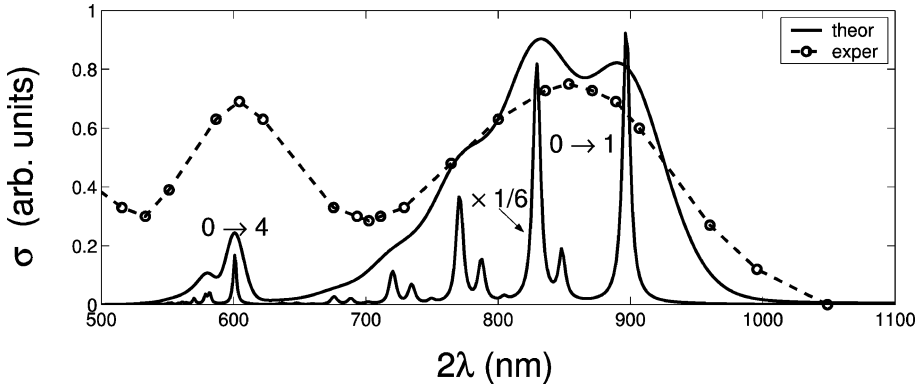

Figure 3. One-photon absorption spectrum of N101. Solid lines display the theoretical spectra calculated for $\Gamma_{10}^{R} = \Gamma_{40}^{R} = 0.01$ eV and $\Gamma_{10}^{R} = 0.05$ eV, $\Gamma_{40}^{R} = 0.025$ eV. Experimental spectra taken from ref 3.

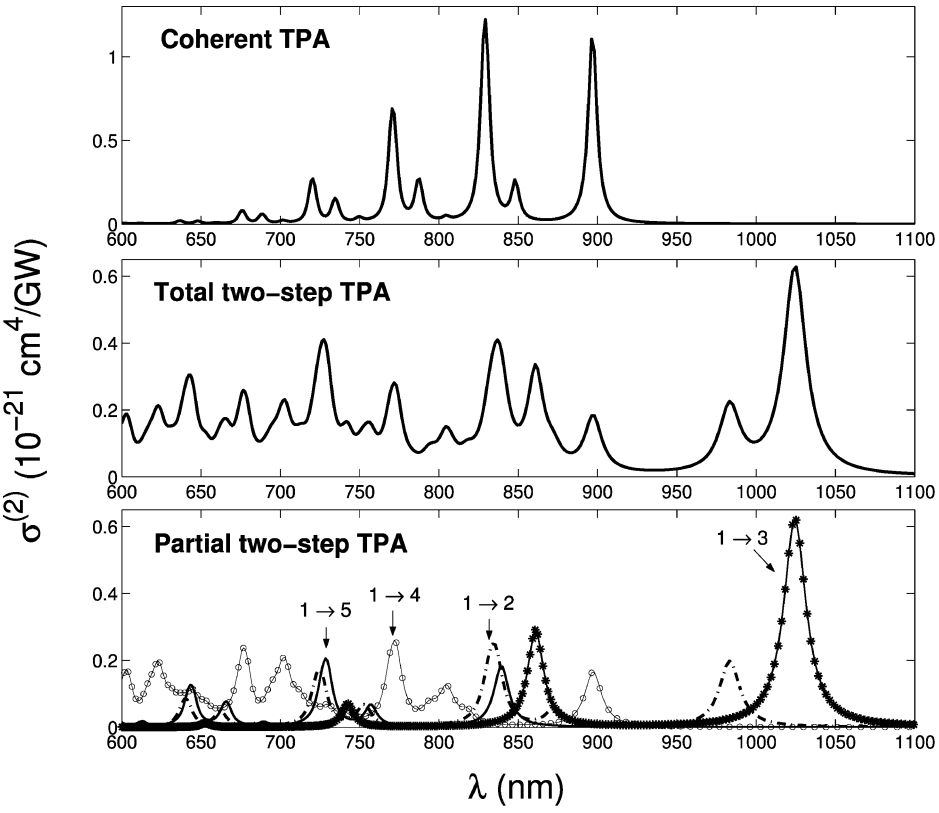

Figure 4. Coherent and partial two-step TPA cross-sections of the N101 molecule. $\Gamma_{10}^{R} = \Gamma_{\alpha 1}^{R} = 0.01$ eV; $\tau\Gamma_{10}^{NR} = 10$. The lowest panel displays the partial two-step TPA cross-sections for the four channels $0 \rightarrow 1 \rightarrow \alpha$, whereas the mid panel shows the total two-step TPA cross-section.

TABLE 4: Frequencies of the Vibrational Modes Included in Our Simulations of the N101 Spectra

mode	66	86	88	90	92	93	100	105	119	121	122	123
ω_q (eV)	0.134	0.153	0.158	0.159	0.161	0.161	0.177	0.181	0.222	0.223	0.224	0.230

$\equiv \Delta d_{11} = -1.94$ au, $\Delta d(40) \equiv \Delta d_{44} = 0.947$ au, $\Delta d(41) = 2.887$ au, $\Delta d(51) = 1.61$ au, $\Delta d(21) = 1.816$ au, and $\Delta d(31) = 0.79$ au. In general, the broadening is not a linear function of the squared change of the solute−solvent potential. Because of this fact, the above choice of spectral line broadening is rather arbitrary.

A comparison of the experimental one- and two-photon absorption spectra (Figures 3 and 5) shows that contrary to the two-photon profile the one-photon spectrum does not display any vibrational structure. This in agreement with our choice of large broadening for the $0 \rightarrow 1$ transition (compared to the excited-state absorption), which smears out the vibrational structure in the one-photon spectrum.

4. Results of Simulations of the N101 Molecule

The results of the simulations of one- and two-photon absorption of the N101 molecule are shown in Figure 3 and Figures 4 and 5, respectively. The one-photon absorption spectrum, Figure 3, consists of two electrovibrational bands related to the transitions to the first ($0 \rightarrow 1$) and fourth ($0 \rightarrow 4$) electronic states. This is in agreement with the experiment,[3] although the intensity of the shortwave band, $0 \rightarrow 4$, is weaker than that observed. Calculations show that the contributions of other electronic states are negligibly small. The wavelength in the one-photon spectrum is doubled in order to facilitate comparison of the one- and two-photon profiles.

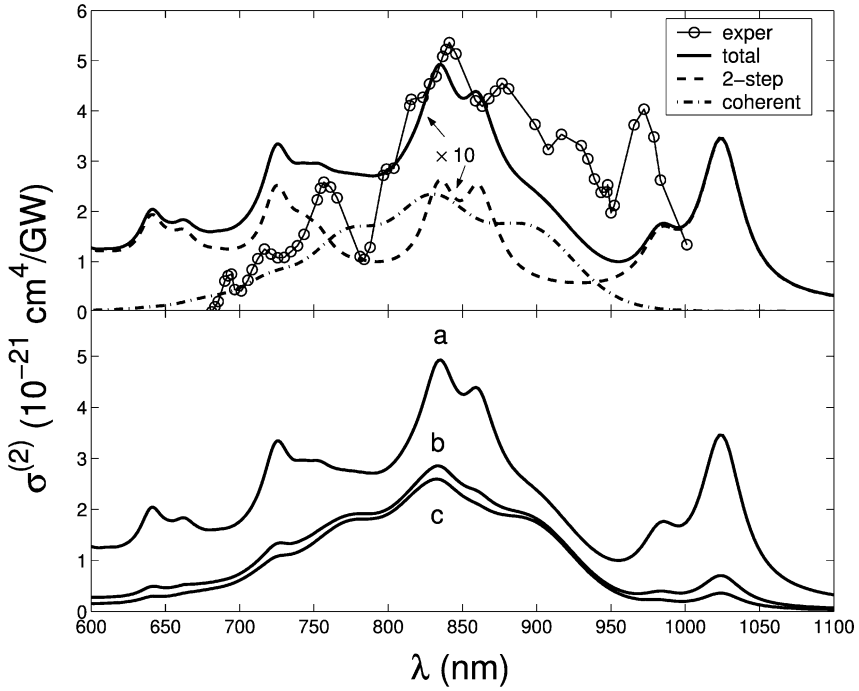

Figure 5. Total spectrum of TPA absorption of the N101 molecule. $\Gamma_{10}^{R} = 0.05$ eV, $\Gamma_{31}^{R} = 0.02$ eV, $\Gamma_{51}^{R} = \Gamma_{21}^{R} = 0.04$ eV, $\Gamma_{41}^{R} = 0.08$ eV, and τ $\Gamma_{10}^{NR} = 10$. The simulated total, coherent, and two-step cross-sections are enlarged 10 times. Experimental spectra taken from ref 3. Upper panel: $P_{10}^{NR}/P_{10}^{R} = 10^{-4}$. Lower panel: $P_{10}^{NR}/P_{10}^{R} = 10^{-4}$ (a), $P_{10}^{NR}/P_{10}^{R} = 2 \times 10^{-5}$ (b), $P_{10}^{NR}/P_{10}^{R} = 10^{-5}$ (c).

The vibrational profiles of the $0 \rightarrow 1$ and $0 \rightarrow 4$ coherent TPA spectra coincide with the vibrational profiles of one-photon absorption (Figure 3). However, contrary to the one-photon spectrum, the coherent TPA profile (Figure 4) is formed mainly because of the $0 \rightarrow 1$ TPA transition. The reason for this is that the TPA cross-section of the $0 \rightarrow 4$ transition ($\propto(d_{40}\Delta d_{44}\langle\nu_4|0_0\rangle)^2$) is much smaller than the $0 \rightarrow 1$ TPA cross-section ($\propto(d_{10}\Delta d_{11}\langle\nu_1|0_0\rangle)^2$) (see Table 1).

The other reason for the distinction of the TPA spectrum from the spectrum of one-photon absorption is the two-step or excited-state absorption, which modifies the TPA profile considerably, see Figure 5. The two-step spectrum is formed by four channels of excited-state absorption, $1 \rightarrow 2$, $1 \rightarrow 3$, $1 \rightarrow 4$, and $1 \rightarrow 5$. As one can see from the simulations (Figures 4 and 5), the two-step TPA contribution has a large vibrational broadening. In agreement with the experiment,[3] the total TPA profile is red-shifted because of the two-step channel.

Figure 5 shows that the TPA spectrum is sensitive to the ratio of nonresonant to resonant one-photon absorption probabilities P_{10}^{NR}/P_{10}^{R}. In the present article, we show the importance of the two-step TPA process caused by nonresonant population of the first excited state. The excited-state absorption due to resonant TPA population of the first excited state also starts influencing the spectral shape of the nonlinear absorption when the intensity of the light is larger than 0.1 GW/cm^2.

It is worth commenting on the energy conservation law in off-resonant one-photon absorption. The resonant frequency between the ground and the first excited electronic state depends strongly on the distance between the absorbing molecule and the solvent molecules. According to the theory of spectral line wings,[13] the one-photon absorption takes place for such an intermolecular distance where the condition of the resonance occurs.

It should be noted that a strong laser field can result in a photomodification of the molecules, the effect of which also leads to the change of the absorption spectrum. This effect is beyond the scope of our article.

5. Summary

The present work addressed the band-shape formation in two-photon spectra and was aimed, in particular, at explaining the origin of differences in band shapes between these spectra and their one-photon counterparts. We have used the experimentally studied N101 [*p*-nitro-*p*′-diphenylamine stilbene] molecule as an illustrative case for this purpose. We have shown that the spectrum of one-photon absorption of the N101 molecule consists of two vibrationally broadened bands related to the transitions to the first and second excited electronic states. The vibrational profile of the second electronic state displays larger vibrational broadening. This, as well as the smaller value of the transitional dipole moment, explains the smaller intensity of the second band. Our simulations of coherent two-photon absorption show strong suppression of the short wavelength band compared to one-photon absorption. This is because the relative two-photon cross-section of the second band is much smaller than the relative intensity of the one-photon absorption. The experimental spectra show similar behavior except for a larger broadening of the first band. To explain this discrepancy, we calculated the two-photon spectrum also taking into account two-step two-photon absorption. The existence of 146 vibrational modes in the studied N101 molecule makes computations very expensive. To overcome this computational problem, we selected only vibrational modes with Huang−Rhys parameters larger than 0.1.

Our simulations show that the contribution of the two-step, or sequential process, is comparable with the coherent one-step two-photon absorption and that the vibrational spectrum of sequential TPA leads to a shift of the spectral profile relative to the one-photon spectrum. We take this as yet another indication of the need to consider off-resonant stepwise contributions even when operating at resonant conditions for the coherent multiphoton excitation.

Acknowledgment. This work was supported by the Swedish Research Council (VR).

References and Notes

(1) Honig, B.; Jortner, J. *J. Chem. Phys.* **1967**, *47*, 3698.

(2) Macak, P.; Luo, Y.; Norman, P.; Ågren, H. *Chem. Phys. Lett.* **2000**, *330*, 447.

(3) Lin, T.-C.; He, G. S.; Prasad, P. N.; Tan, L.-S. *J. Mater. Chem.* **2004**, *14*, 982.

(4) He, G. S.; Lin, T.-C.; Dai, J.; Prasad, P. N. *J. Phys. Chem.* **2004**, *120*, 5275.

(5) He, G. S.; Swiatkiewicz, J.; Jiang, Y.; Prasad, P. N.; Reinhardt, B. A.; Tan, L.-S.; Kannan, R. *Opt. Express* **2002**, *10*, 566.

(6) He, G. S.; Lin, T.-C.; Prasad, P. N.; Kannan, R.; Vaia, R. A.; Tan, L.-S. *J. Phys. Chem. A* **2000**, *104*, 4805.

(7) Baier, J.; Pösch, P.; Jungmann, G.; Schmidt, H.-W.; Seilmeier, A. *J. Chem. Phys.* **2001**, *114*, 6739.

(8) Gel'mukhanov, F.; Baev, A.; Macak, P.; Luo, Y.; Ågren, H. *J. Opt. Soc. Am. B* **2002**, *19*, 937.

(9) Baev, A.; Gel'mukhanov, F.; Macak, P.; Luo, Y.; Ågren, H. *J. Chem. Phys.* **2002**, *117*, 6214.

(10) Baev, A.; Gel'mukhanov, F.; Rubio-Pons, O.; Cronstrand, P.; Ågren, H. *J. Opt. Soc. Am. B* **2004**, *21*, 384.

(11) Baev, A.; Rubio-Pons, O.; Gel'mukhanov, F.; Ågren, H. *J. Phys. Chem. A* **2004**, *108*, 7406.

(12) Baev, A.; Kimberg, V.; Polyutov, S.; Gel'mukhanov, F.; Ågren, H. *J. Opt. Soc. Am. B* **2005**, *22*, 385.

(13) Allard, N.; Kielkopf, J. *Rev. Mod. Phys.* **1982**, *54*, 1103.

(14) Marcus, R. A. *J. Chem. Phys.* **1965**, *43*, 1261.

(15) Shemetulskis, N. E.; Loring, R. F. *J. Chem. Phys.* **1991**, *95*, 4756.

(16) Matyushov, D. V.; Ladanyi, B. M. *J. Chem. Phys.* **1997**, *107*, 1375.

(17) Rumi, M.; Ehrlich, J. E.; Heikal, A. A,; Perry, J. W.; Barlow, S.; Hu, Z.; McCord-Maughon, D.; Parker, T. C.; Röckel, H.; Thayumanavan, S.; Marder, S. R.; Beljonne, D.; Brédas, J.-L. *J. Am. Chem. Soc.* **2000**, *122*, 9500.

(18) Turro, N. J. *Modern Molecular Photochemistry*; Benjamin: New York, 1978.

(19) Kamada, K., submitted for publication.

(20) Chung, S.-J.; Kim, K.-S.; Lin, T.-C.; He, G. S.; Swiatkiewicz, J.; Prasad, P. N. *J. Phys. Chem. B* **1999**, *103*, 10741.

(21) *DALTON, A Molecular Electronic Structure Program*, Release 2.0; 2005; see http://www.kjemi.uio.no/software/dalton/dalton.html